A cell migration device that maintains a defined surface with no cellular damage during wound edge generation†

Michael Robert Doran,[a] Richard James Mills,[a] Anthony James Parker,[b] Kerry Anne Landman[c] and Justin John Cooper-White*[a]

Received 15th January 2009, Accepted 29th April 2009
First published as an Advance Article on the web 14th May 2009
DOI: 10.1039/b900791a

Studying the rate of cell migration provides insight into fundamental cell biology as well as a tool to assess the functionality of synthetic surfaces and soluble environments used in tissue engineering. The traditional tools used to study cell migration include the fence and wound healing assays. In this paper we describe the development of a microchannel based device for the study of cell migration on defined surfaces. We demonstrate that this device provides a superior tool, relative to the previously mentioned assays, for assessing the propagation rate of cell wave fronts. The significant advantage provided by this technology is the ability to maintain a virgin surface prior to the commencement of the cell migration assay. Here, the device is used to assess rates of mouse fibroblasts (NIH 3T3) and human osteosarcoma (SaOS2) cell migration on surfaces functionalized with various extracellular matrix proteins as a demonstration that confining cell migration within a microchannel produces consistent and robust data. The device design enables rapid and simplistic assessment of multiple repeats on a single chip, where surfaces have not been previously exposed to cells or cellular secretions.

Introduction

Cellular interactions with surfaces influence cell behaviour including migration, proliferation and differentiation.[1,2] Understanding the relative impact of surface treatment on these behaviours is paramount in many tissue engineering applications. In many cases, the development of tissue engineered products relies on functionalizing surfaces with specific proteins or peptides in order to firstly study and thereafter direct cell behaviour.[1] One of the tools utilized in laboratories world wide to study cell migration and surface interactions is the classic wound healing or scrape assay. This assay is performed by creating a "wound" in a cell monolayer and capturing photographic images over time, from the point of "wound" creation until closure. Using data from these images, it is possible to quantify cell migration rates and study cell–cell and cell–matrix interactions.[3] The rate of "wound" closure is in fact the sum of numerous cell processes, including cell migration, proliferation and cell morphology, in response to both soluble and solid substrate influences.[4] Unfortunately, the outcomes of the wound healing assay are somewhat confounded by the following four factors: (1) in the process of generating the "wound", the underlying matrix of specific ligands may be removed or, alternatively, the matrix secreted by the previously existing cell monolayer may remain following the scrape. In either case, the actual composition of the surface, now termed the "wound", is ambiguous; (2) the thickness of the wound may vary along its length and is known to be a function of the tool dimension as well as the force and velocity used in making the wound; (3) the relative cell confluence in the area where the "wound" is created undoubtedly influences the outcome; (4) the act of creating the wound destroys and damages cells on the initial wave front, which in some cases actually results in the cell wave front contracting transiently.[5] As a result of the mentioned deficiencies, the wound healing assay can be an inappropriate tool for the assessment of cell migration rates, especially when evaluating novel surfaces which will either be damaged or fouled as an artefact of this assay.

The previous decade has seen significant advancements in the development of microdevices designed to assess cell migration. Poujade *et al.* developed a polydimethyl siloxane (PDMS) based stencil tool for evaluating cell migration, which overcomes many of the problems associated with the classical wound healing assay.[6] However, even this eloquent solution potentially compromises surface composition by the fact that the PDMS stencil must be fixed on top of the virgin surface until the cell monolayer is established. Nie *et al.* developed a microfluidic device where the laminar flow of trypsin generates a well-defined wound edge.[7] While this method elicits only minor damage to cells on the wound edge, the surface onto which the cells will migrate remains ambiguous. A microfluidic based device proposed by Chung *et al.* enables the assessment of cell migration through gel scaffolds in response to soluble gradients.[8] Wang *et al.* have developed a device where the wound edge is generated using a self-assembled monolayer which inhibits cell adhesion.[9] When current is applied, the monolayer is desorbed, making the surface available for cell attachment and migration. This device is best suited for assessing the influence soluble molecules have on cell migration rather than cell–surface interactions. Kaji *et al.*

[a]*Australian Institute for Bioengineering and Nanotechnology, University of Queensland, Queensland, 4072, Australia. E-mail: j.cooperwhite@uq.edu.au*
[b]*Institute of Health and Biomedical Innovation (ihbi), University of Technology Queensland, Queensland, 4059, Australia.*
[c]*Department of Mathematics and Statistics, University of Melbourne, Victoria, 3010, Australia.*
† The authors would like to thank the Australian Research Council Discovery Grant Scheme for funding this work.

study the interaction of two cells in co-culture where each cell type is established in monolayer on a separate chip prior to initiation of the study.[10] The chips are brought together such that the two cell monolayers are in contact and in the same plane. This unique system permits the study of cell behaviour in response to an adjacent monolayer of cells of a different phenotype.

In studying how cell–surface interactions influence cell migration, it is critical that the migration surface is not fouled with cell debris, nor physically damaged by mechanical scraping or enzymatic degradation, prior to cellular interactions. In this article we describe a microfabricated device that permits the study of cell migration on virgin surfaces in microchannels. Virgin surfaces are maintained in microchannels which branch off a central main culture chamber. The dimensions of the microchannel coupled with the material and fluid properties prevent medium from the culture chamber entering the microchannels. This enables both the maintenance of the virgin surface within the channel during the establishment of a monolayer within the main chamber and the development of a "wound edge" at the chamber–channel interface. As the monolayer in the main chamber simply expands to this interface, there is no cellular damage in the generation of the wound edge. The microchannel is then backfilled with culture medium, connecting the channel with the main chamber and enabling the migration process to begin. This novel device format thus overcomes many of the deficiencies associated with the previously mentioned assay formats aimed at studying cell migration as a function of cell–surface interaction.

In this paper, we outline preliminary experiments which demonstrate that the described device design functions to maintain a virgin surface for cell migration and generates highly reproducible data. This migration data is then used to estimate specific cell–surface diffusion coefficients for NIH 3T3 fibroblasts and human osteosarcoma SaOS2 cells on surfaces functionalized with a number of different matrix molecules.

Materials and methods

For clarity, materials and methods has been subdivided such that individual sections describe device design and fabrication, cell culture and mathematical methods for determination of characteristic cell diffusion coefficients.

Multichannel migration device (MMD) design and fabrication

Fig. 1 shows the multichannel migration device (MMD) which enables the simultaneous observation of multiple repeats of cell migration down microchannels onto virgin surfaces. The key feature of this device is that a confluent cell monolayer can be established within the main chamber without any cell migration or medium flow into the microchannels until they are backfilled with medium through the syringe ports. This feature allows the maintenance of a *virgin* surface within the channel despite the culture of cells at the channel–main chamber interface. Isolation of the channels from the main chamber is achieved by tailoring the device material composition and channel dimension such that fluid surface tension does not allow fluid to flow from the main chamber into the unfilled channels. Only when the channel is backfilled with fluid is there a direct fluid connection between the channel and main chamber.

Device fabrication

In all cases, channels were constructed from polydimethylsiloxane (PDMS, Sylgard 184, Dow Corning) using soft lithography[11] and bonded to a glass (Proscitech, Australia) base which provides the substrate for protein adhesion and subsequent cell attachment. In brief, an SU-8 photo resist (SU8-2025, MicroChem) mould was used to cast channels into PDMS which was then bonded to glass *via* plasma activation of the PDMS surface. The channel depth is 100 μm in all cases. The PDMS layer is 5 mm thick. In standard culture cell, medium is often 5 mm in depth and, as the solubility of oxygen in PDMS is approximately an order of magnitude grater than that of water, we assume that gas transfer to cells in the migration channels is not a limiting factor.[12] The device is sterilized prior to surface modification with proteins and cell culture by steam sterilization at 121 °C for 20 min.

Surface functionalization

The glass surfaces, which form the base of the microchannels, were functionalized by allowing extracellular matrix (ECM) molecules to physisorb out of the solution onto the glass substrate over night at 4 °C. ECM molecules were solubilized in phosphate buffered saline (PBS) as follows: 50 μg ml^{-1} collagen I (C3867 Sigma-Aldrich St. Louis, MO, USA), 50 μg ml^{-1} collagen IV (C5533 Sigma-Aldrich St. Louis, MO, USA), 2% BSA (A8806 Sigma-Aldrich St. Louis, MO, USA) or 100% FBS (Bio-Whittaker Walkersville, MD, USA).

Duplicate migration surfaces having had a physisorbed layer of either collagen I, collagen IV or FBS were treated with a 2% BSA solution for 2 h at 20 °C to "block" or prevent any further non-specific binding to the glass substrate. Following the adsorption or blocking process, channels were evacuated of matrix molecules or BSA suspension fluid.

Identical surfaces were generated on separate 1 cm^2 glass plates (sections generated from the same glass as utilized in the base of the devices) for the evaluation of cell attachment, spreading and doubling time on each surface.

Cell culture

Human osteosarcoma cells, SaOS2 cells, were cultured in DMEM F-12 (Gibco/Invitrogen Carlsbad, CA, USA) plus 10% FBS. Mouse NIH 3T3 fibroblasts were cultured in DMEM (Gibco/Invitrogen Carlsbad, CA, USA) plus 10% FBS (Serum Supreme, BioWhittaker Walkersville, MD, USA). All medium was supplemented with penicillin/streptomycin (10 000 units Gibco/Invitrogen Carlsbad, CA, USA). Cultures were maintained at 37 °C in a 5% CO_2 incubator. Measurement of migration distance was performed using an Olympus CKX41 microscope and Q Capture Pro software.

Cell migration rates on surfaces composed of various matrix molecules were studied using the MMD. The tailored surfaces in the MMDs were established as described previously. A cell suspension (10^7 cells ml^{-1}) was loaded into the main chamber of the device. Cells were incubated over night at 37 °C and 5% CO_2

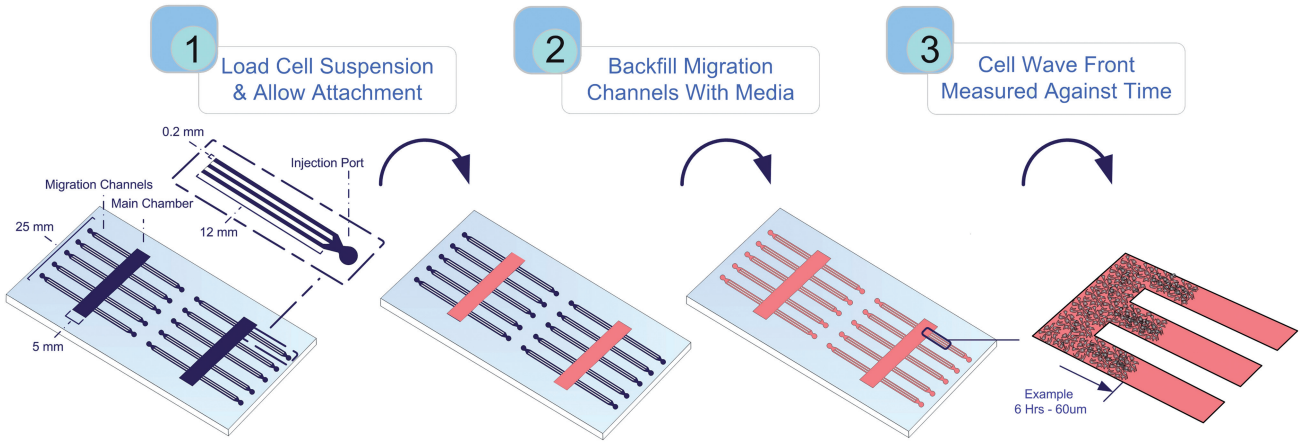

Fig. 1 The figure shows the dimensions of the MMD. The main chamber and channels are cast from PDMS while the base is glass. The main chamber is open at the top allowing direct loading of medium and cell inoculum into this space from above with a pipette. Each set of three channels branching off the main chamber converge at a single injection port. (1) A confluent cell monolayer (medium represented by red) is established within the main chamber by direct loading into this portion of the device *via* pipette. Medium does not enter the channels branching off the main chamber, as surface tension prevents spontaneous flow down the channel opening (200 × 100 μm). (2) After having established a confluent monolayer, within the main chamber, the channels are backfilled with medium, using a blunt ended syringe, *via* the injection ports. This action makes the channels continuous with the main chamber and open to cell migration. (3) Cell migration or the progression of the cell wave front down the microchannels is recorded at regular time intervals.

to establish a monolayer and non-adherent cells were removed from the main chamber by exchanging the main chamber medium volume 2–3 times. The migration channels were then backfilled and time zero pictures taken. Cell migration photographs and measurements were taken at 18, 24 and 36 h.

On replica surfaces (on glass 1 cm^2 glass plates), cell adhesion, spread area and doubling time were assessed. Cell adhesion and spread area were assessed at 4 h while doubling time was assessed over a 48 h period. Cell spread area was assessed using ImageJ software (NIH).

Cell migration and estimation of diffusion coefficients

The propagation of the cell wave front down the microchannel is a function of the cell spread area, doubling time and characteristic diffusion coefficient. We have utilized the Fisher equation to enable us to relate these variables and back calculate the characteristic diffusion coefficient for each cell–surface combination using measured values for the wave front velocity, cell spreading area and doubling time.

Many models of cell migration[13,14,15,16] are based on the Fisher equation, which describes the cell front as a travelling wave of fixed shape moving at constant velocity as a function of cell proliferation rate and a characteristic diffusion constant. This relationship is described mathematically in eqn (1):[15]

$$\frac{\partial c}{\partial t} = \nabla\cdot(D\nabla c) + \lambda\left(1 - \frac{c}{c_{\max}}\right)c \qquad (1)$$

Cell density is defined by the variable c (cells cm^{-2}), D is the characteristic cell diffusion constant, λ (s^{-1}) is the unrestricted growth rate, while c_{max} (cells cm^{-2}) is the cell density at confluence. The first term on the right hand side of the equation represents cell migration by diffusion, as a result of random walks, while the second term represents cell proliferation by logistic growth.

In order to determine the characteristic diffusion constant for a particular cell–surface combination, we use the relationship derived from the Fisher equation for migration in one spatial dimension:[13,14,16]

$$v = 2\sqrt{D\lambda} \qquad (2)$$

where v is the cell wave front velocity (cm s^{-1}) and $\lambda = \ln 2/T$, where T is the cell doubling time.

Results and discussion

Results and discussion are subdivided first discussing cell migration down channels on defined surfaces, then proliferation and spread area, and finally determination of characteristic cell diffusion coefficients on each of these surfaces.

Migration on defined surfaces

Fig. 2 shows, as an example, the view of 3T3 cell migration within the MMD. We observe that the cell wave front maintains a well-defined shape even after 48 h. The results of NIH 3T3 mouse fibroblast and SaOS2 human osteosarcoma migration on surfaces functionalized with either collagen I, collagen IV, BSA or FBS within the MMD are shown in Fig. 3 and 4, respectively.

Fig. 3 shows the resulting NIH 3T3 fibroblast wave front propagation on various ECM molecules. The highest NIH 3T3 fibroblast migration rate of approximately 11 μm h^{-1} was observed on surfaces composed of untreated glass, collagen I, FBS and FBS blocked with BSA (all statistically equivalent). The collagen IV surfaces generated an intermediate migration rate, which differed from any other surface in this study ($P < 0.05$). Surfaces treated with BSA or collagen I or IV surfaces blocked with BSA produced the slowest rates, of approximately 5 μm h^{-1} (all statistically equivalent). The reduced migration rate observed

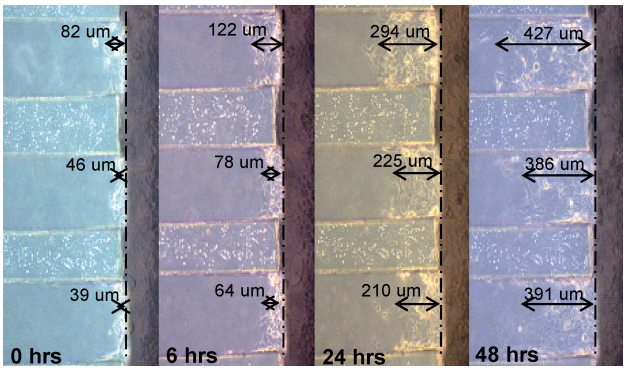

Fig. 2 The figure shows (phase contrast 10× magnification) NIH 3T3 fibroblast cell migration along 3 adjacent 200 μm channels in the MMD. The arrows show how cell migration is tracked from the base or channel origin to the edge of the cell wave front. The leading edge of cell migration is defined in this case as the average distance between the leading and lagging cell on the wave front.

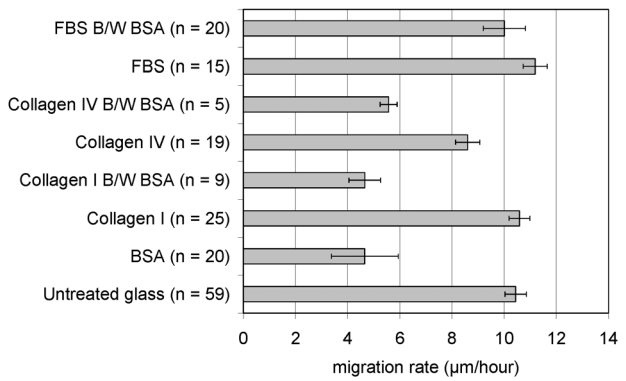

Fig. 3 The plot contrasts relative NIH 3T3 fibroblast cell front velocities on surfaces functionalized with various ECM molecules. Each bar represents an average of n measurements, while error bars reflect the standard error of the mean.

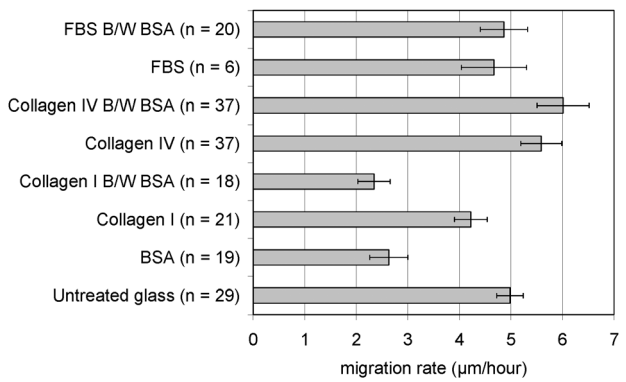

Fig. 4 The plot contrasts relative SaOS2 osteosarcoma cell front velocities on surfaces functionalized with various ECM molecules. Each bar represents an average of n measurements, while error bars reflect the standard error of the mean.

on the collagen surfaces blocked with BSA was unexpected and will be discussed further in the next section.

The NIH 3T3 fibroblast migration rates of approximately 11 μm h^{-1} reported here, for serum-coated surfaces, are lower than that observed for 3T3 migration when cultured at low density. For example, NIH 3T3 cells have been previously observed to migrate at rates of 40 μm h^{-1}, while mouse embryonic fibroblasts have been shown to have a migration rate of approximately 50 μm h^{-1}.[17,18] Cell migration velocities at low cell densities[17,18] were determined by taking images at much shorter time points using time-lapse imaging, while our data reflects the net migration of high-density cell wave front measured only at 18, 24 and 36 h time points. It has been shown that cell migration rates are reduced at high cell densities and that NIH 3T3 cell migration rates are reduced from an average of 37 μm h^{-1} to an average of 12 μm h^{-1} when observations are made at low and high cell density, respectively.[19] Furthermore, NIH 3T3 cell wave front migration rates of 30 μm h^{-1} are observed on wave fronts having a much more diffuse pattern of cells than wave fronts observed in the MMD, where wave fronts are very square and cells tightly packed.

Fig. 4 shows SaOS2 osteosarcoma cell wave front propagation on various surfaces. Wave front velocities on untreated glass, collagen I, collagen IV, collagen IV blocked with BSA, FBS and FBS blocked with BSA were all statistically equivalent. Rates were reduced on surfaces treated with either BSA or collagen I blocked with BSA ($P < 0.05$). Interestingly, blocking collagen IV surfaces with BSA did not inhibit SaOS2 in the same way that it did with NIH 3T3 cells.

The maximal wave front propagation rates observed for SaOS2 human osteosarcoma was approximately 5.5 μm h^{-1}, in contrast to the 11 μm h^{-1} observed for the NIH 3T3 fibroblasts.

Characteristic diffusion coefficients

Utilizing the Fisher equation, as described in the methods, it is possible to estimate the diffusion coefficient from measured values of the wave front velocity and cell doubling time (see eqn (2)). Doubling times for NIH 3T3 and SaOS2 cells on the various surfaces are shown in Table 1. The average doubling time for NIH 3T3 and SaOS2 cells were observed to be 21.4 ± 2.8 and 38.8 ± 3.1, respectively. These doubling times were found to be statistically equivalent on all surfaces (ANOVA) and to be equivalent to published values.[20–22] We were surprised that doubling times did not vary more significantly on various surfaces and hence investigated this in more detail.

We hypothesize that the surfaces investigated here do not significantly influence cell doubling times, as physisorption of ECM molecules onto the glass substrate does not produce a surface which excludes alternate ligand binding. This hypothesis is supported by the fact that cell attachment and spreading on glass surfaces is not blocked with BSA, which indicates that BSA is either being competitively desorbed or that it did not completely cover the surface initially, leaving gaps filled by FBS medium components. Fig. 5 provides evidence, particularly in 5A, where the presence of serum blocking with albumin does not hinder cell attachment. Fig. 6 provides additional information on cell spread area on each of the surfaces. The variable spread area, like the migration rate (Fig. 3 and 4), indicate that while the

Table 1 The table lists cell doubling times on various surfaces. Listed values are the average of 3 replicates plus or minus standard deviation

Surface	NIH 3T3 doubling time/h	SaOS2 doubling time/h
Untreated	21.4 ± 1.7	37.8 ± 4.4
BSA	23.3 ± 1.9	40.1 ± 4.9
Collagen I	22.1 ± 2.1	39.4 ± 2.4
Collagen I W/BSA	21.0 ± 1.5	39.1 ± 3.7
Collagen IV	20.9 ± 1.9	38.0 ± 4.4
Collagen IV W/BSA	19.3 ± 1.8	37.1 ± 2.8
FBS	20.3 ± 0.5	40.2 ± 2.9
FBS W/BSA	22.6 ± 2.0	38.6 ± 2.7
Average	*21.4 ± 2.8*	*38.8 ± 3.1*

Table 2 Characteristic diffusion coefficients on different surfaces generated using wave front velocities and doubling times

Surface	NIH 3T3 diffusion coefficient/cm^2 s^{-1}	SaOS2 diffusion coefficient/cm^2 s^{-1}
Untreated	$2.5 \pm 0.2 \times 10^{-9}$	$1.0 \pm 0.1 \times 10^{-9}$
BSA	$0.8 \pm 0.3 \times 10^{-9}$	$0.4 \pm 0.1 \times 10^{-9}$
Collagen I	$2.6 \pm 0.2 \times 10^{-9}$	$0.8 \pm 0.1 \times 10^{-9}$
Collagen I W/BSA	$0.5 \pm 0.01 \times 10^{-9}$	$0.3 \pm 0.7 \times 10^{-9}$
Collagen IV	$1.6 \pm 0.2 \times 10^{-9}$	$1.4 \pm 0.2 \times 10^{-9}$
Collagen IV W/BSA	$0.6 \pm 0.1 \times 10^{-9}$	$1.7 \pm 0.3 \times 10^{-9}$
FBS	$2.6 \pm 0.2 \times 10^{-9}$	$1.0 \pm 0.2 \times 10^{-9}$
FBS W/BSA	$2.5 \pm 0.4 \times 10^{-9}$	$0.8 \pm 0.2 \times 10^{-9}$

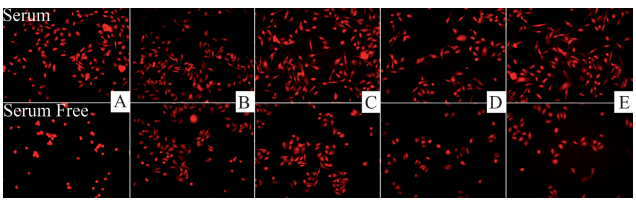

Fig. 5 NIH 3T3 fibroblast attachment after 4 h incubation on surfaces of (A) albumin, (B) collagen I, (C) collagen I blocked with BSA, (D) collagen IV and (E) collagen IV blocked with BSA.

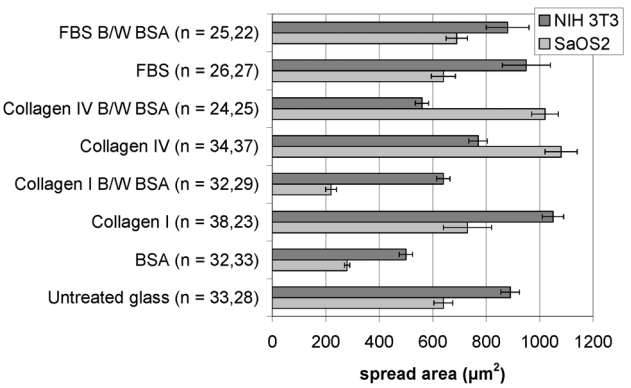

Fig. 6 NIH 3T3 and SaOS2 cell spread area on glass surfaces functionalized with various ECM proteins. Number of replicates indicated by *n*, error bars reflect standard error of the mean.

ECM molecules physisorbed onto the glass may not exclusively dictate cell behaviour, they most certainly influence cell spread area and migration rate.

Despite the variable spread areas shown in Fig. 6, it is still possible to relate the characteristic diffusion coefficient (as described in eqn (2)) back to only wave front velocity and cell doubling time, as this relation assumes that the surfaces behind the wave front are at carrying capacity, which is certainly the case in our system. Thus, utilizing the measured doubling times listed in Table 1, it is possible to estimate the diffusion coefficients for any of the cell–surface combinations (listed in Table 2).

Estimated motility coefficients derived for both cell lines correlated well with values from the literature for similar cell lines and surfaces.[13–15,23,24] For example, neonatal rat osteoblasts on various peptide motif (RGDS, RDGS) modified glass substrates have been reported to have diffusion coefficients ranging from 1.22–2.33 $\times$ 10^{-9} cm^2 s^{-1}.[23] Maini *et al.*,[13,14] also showed the difference in cell motility on different surfaces using human peritoneal mesothelial cells. A diffusion coefficient of 4.17×10^{-9} cm^2 s^{-1} on an untreated surface was estimated, while on a collagen IV surface it was approximately double that at 9.18×10^{-9} cm^2 s^{-1}. It should be noted that diffusion coefficients an order of magnitude higher have been reported on glass, typically using the highly motile Leukocyte cell lines.[15]

NIH 3T3 cells within the current study showed higher diffusion coefficients compared with the SaOS2 cells. The diffusion coefficients follow the same statistical trend as shown in the measured migration rates (see Fig. 3 and 4), which is expected as doubling times were found to be similar in all cases. This shows definitively that NIH 3T3 cells diffuse/migrate fastest over untreated glass, collagen I, FBS and FBS blocked with BSA. Intermediate diffusion coefficients are produced on collagen IV and the slowest values were recorded on surfaces treated with BSA or collagen I or IV surfaces blocked with BSA. SaOS2 cells diffused fastest on surfaces having compositions which were either composed of untreated glass, collagen I, collagen IV, collagen IV blocked with BSA, FBS and FBS blocked with BSA, with values reduced on surfaces treated with either BSA or collagen I blocked with BSA.

Conclusions

Cell migration assays are a valuable tool for gaining insight into cell behaviour as a function of surface chemistry and often soluble cues. When utilizing migration assays to assess cell interaction with surfaces, experimental outcomes are often compromised by the inability to maintain a virgin surface or defined surface chemistry prior to the initiation of the migration event. This occurs as either medium containing cellular secretions or cells themselves will have come into contact with the surface prior to the initiation of the migration event. In an effort to overcome this ambiguity, we have developed a multichannel migration device which enables the generation of a defined surface void of culture medium or any cell contact up till the point at which the migration assay is initiated.

In this novel system, cells migrate from a central culture chamber down microchannels. Due to the material composition and dimensions of the microchannels, surface tension prevents fluid from invading the channels from the main culture chamber, thus maintaining their virgin surface. Once the cell layer in the

main chamber is confluent, the process of migration down the channels is initiated by backfilling the channels, thus providing a fluid connection with the main chamber. In this paper we describe the design, fabrication and use of this multichannel migration device to investigate wave front propagation rates and characteristic cell diffusion rates on surfaces functionalized with various ECM molecules.

Experimental results show that NIH 3T3 wave front propagation and diffusion coefficients are greatest on surfaces composed of untreated glass, collagen I, FBS and FBS blocked with BSA. SaOS2 osteosarcoma cell wave front propagation and diffusion coefficients are greatest on surfaces composed of collagen I, collagen IV, collagen IV blocked with BSA, FBS and FBS blocked with BSA.

The multichannel migration device shown here provides a rapid and robust tool for the evaluation of the influence surface biochemistry has on cell migration. While not within the scope of this paper, we have also utilized this device to assess cell migration in response to soluble factors and again found it to provide rapid and reproducible results. We believe that the underlying concept described here, which enables the maintenance of a virgin surface prior to any cell contact, represents a significant advancement in cell migration assessment technologies.

References

1 M. P. Lutolf and J. A. Hubbell, *Nat. Biotechnol.*, 2005, **23**, 47–55.
2 H. Shin, S. Jo and A. G. Mikos, *Biomaterials*, 2003, **24**, 4353–4364.
3 L. Rodriguez, X. Wu and J. Guan, *Methods Mol. Biol.*, 2005, **294**, 23–29.
4 A. Q. Cai, K. A. Landman and B. D. Hughes, *J. Theor. Biol.*, 2007, **245**, 576–594.
5 H. Thielecke, Impidjati and G. R. Fuhr, *J. Phys.: Condens. Matter*, 2006, **18**, S627–S637.
6 M. Poujade, E. Grasland-Mongrain, A. Hertzog, J. Jouanneau, P. Chavrier, B. Ladoux, A. Buguin and P. Silberzan, *Proc. Natl. Acad. Sci. U. S. A.*, 2007, **104**, 15988–15993.
7 F. Q. Nie, M. Yamada, J. Kobayashi, M. Yamato, A. Kikuchi and T. Okano, *Biomaterials*, 2007, **28**, 4017–4022.
8 S. Chung, R. Sudo, P. J. Mack, C. R. Wan, V. Vickerman and R. D. Kamm, *Lab Chip*, 2009, **9**, 269–275.
9 L. Wang, J. Zhu, C. Deng, W. Xing and J. Cheng, *Lab Chip*, 2008, **8**, 872–878.
10 H. Kaji, T. Yokoi, T. Kawashima and M. Nishizawa, *Lab Chip*, 2009, **9**, 427–432.
11 S. K. Sia and G. M. Whitesides, *Electrophoresis*, 2003, **24**, 3563–3576.
12 J. M. Baltz and J. D. Biggers, *Mol. Reprod. Dev.*, 1991, **28**, 351–355.
13 P. K. Maini, D. L. S. McElwain and D. I. Leavesley, *Tissue Eng.*, 2004, **10**, 475–482.
14 P. K. Maini, D. L. McElwain and D. I. Leavesley, *Appl. Math. Lett.*, 2004, 575–580.
15 B. G. Sengers, C. P. Please and R. O. C. Oreffo, *J. R. Soc. Interface*, 2007, **4**, 1107–1117.
16 K. Takamizawa, S. Niu and T. Matsuda, *J. Biomater. Sci., Polym. Ed.*, 1996, **8**, 323–334.
17 H. B. Wang, M. Dembo, S. K. Hanks and Y. L. Wang, *Proc. Natl. Acad. Sci. U. S. A.*, 2001, **98**, 11295–11300.
18 K. Webb, V. Hlady and P. A. Tresco, *J. Biomed. Mater. Res.*, 2000, **49**, 362–368.
19 A. Tremel, A. Cai, N. Tirtaatmadja, B. D. Hughes, G. W. Stevens, K. A. Landman and A. J. O'Connor, *Chem. Eng. Sci.*, 2009, **64**, 247–253.
20 J. Fogh, J. M. Fogh and T. Orfeo, *J. Nat. Cancer Inst.*, 1977, **59**, 221–226.
21 J. Fogh, W. C. Wright and J. D. Loveless, *J. Nat. Cancer Inst.*, 1977, **58**, 209–214.
22 J. l. Jainchil, S. A. Aaronson and G. J. Todaro, *J. Virol.*, 1969, **4**, 549.
23 K. C. Dee, T. T. Andersen and R. Bizios, *Biomaterials*, 1999, **20**, 221–227.
24 K. Takamizawa, S. Niu and T. Matsuda, *J. Biomater. Sci., Polym. Ed.*, 1997, **8**, 323–334.